Precision Attitude Determination Using a Multiple Model Adaptive Estimation Scheme

Quang M. Lam
Orbital Sciences Corporation
Dulles, VA
Lam.quang@orbital.com

John L. Crassidis
University at Buffalo
Amherst, NY
johnc@eng.buffalo.edu

Abstract—This paper is mainly motivated by three reasons: (1) future missions which will necessitate the employment of low cost and low grade Micro-Electro-Mechanical Systems (MEMS) sensors (e.g., MEMS gyros or compact star trackers) while still demanding a high precision attitude estimation, (2) development of a real-time noise statistics estimation capability in order to extend/enhance the performance of a traditional Kalman estimator whose performance is mainly dictated by the knowledge accuracy of its process noise and measurement noise covariance matrices, and (3) performance enhancement of a traditional 6 state Extended Kalman Filter (EKF) whose performance is drastically affected and compromised due to its inability to account for scale factor (SF) errors and misalignment errors. Three specific design areas to be investigated in this paper include: (1) the design and implementation of an attitude determination system (ADS) using a Multiple Model Adaptive Estimation (MMAE) scheme wherein the mixing of various EKF models reflecting various state dimensions is employed to accommodate for SF errors and misalignment errors at high rate operating conditions, (2) real-time gyro noise statistics (rate random walk, angular random walk, and SF errors) estimation via an additional MMAE scheme implemented in parallel to provide process noise update to the ADS individual EKF, and (3) the applicability of MMAE scheme to multi-sensor data fusion for an effective measurement update. The feasibility of the proposed concept and its performance improvement as compared to a traditional approach are evaluated via simulation.[1 2]

Table of Contents

1.0 INTRODUCTION

The attitude determination systems (ADS) of the majority of earth observation missions (e.g., EO-1 or GOES N-Q) traditionally employ a six state ADS Kalman filter (e.g., see Lefferts, et al [1]) which calibrates the gyro bias error and star tracker attitude error by fusing both star tracker and gyro data in a "bootstrap" fashion to determine the spacecraft attitude. An ADS filter with a higher dimension state vector is simply not needed for these types of missions because of its low orbit rate, less stringent attitude knowledge requirements, and high quality ADS sensors (i.e., gyros and star trackers selected for these missions are high grade components). As a result, onboard ADS Kalman filters, with a larger dimension state vector applied to the spacecraft attitude determination system, have been rarely observed. Large state dimension ADS filters are normally applied to ground-based software systems for telemetry data processing to fully examine the on-orbit sensor performance.

Stringent attitude knowledge requirements together with spacecraft agility performance specifications demanded by present and future missions have altered such a design tradition and presented a greater design challenge to ADS designers. These include (i) how to separate scale factor errors stability from bias drift stability under high rate operating conditions; (ii) how to achieve precision estimation and accurate tracking of these two parameters when they are strongly correlated at high rate condition; (iii) should a multiple filtering architecture be implemented in a scheduling scheme to address mode variations by having each individual filter turned on based on real-time dynamic mode dependency or should a mix of all filters be employed simultaneously; (iv) what are the design options that ADS designers can use to produce adequate ADS systems meeting stringent performance requirements at milli-arcsec or even micro-arcsec levels while state-of-the art sensing devices such as advanced star trackers only offer a noise equivalent angle (NEA) of 3 arcsec, etc. This paper is intended to address the aforementioned design challenges. Three specific design objectives to be investigated in this paper include: (1) the design and implementation of multiple EKF models mixing to address the spill-over effect of scale factor error stability to gyro bias stability subject to multiple high rate operating conditions, (2) real-time gyro noise estimation for EKF process noise update, and (3) applicability of this hybrid ADS multi-mode situation using a multiple model adaptive attitude estimation (MMAAE) scheme to multiple sensors fusion.

The proposed MMAAE architecture offers two key adaptation design features: (1) variable process noise computation via MMAE scheme implemented in the outer

[1] 1-4244-0525-4/07/$20.00 ©2007 IEEE
[2] IEEEAC paper #1439, Version 8, Updated Dec 8, 2006

loop and (2) variable weighted summation of the attitude correction to effectively produce optimal correction in the Bayesian fusion sense. Missions with large operational rates will benefit from the first feature while the second feature will primarily offer a great solution to any mission that deploys multiple star trackers or precision guidance sensors to meet the extreme precision attitude estimation requirements.

The proposed MMAAE for future ADS applications is also suitable for a parallel implementation in the event of multiple star tracker updates, thus improving the ADS performance far more than the traditional sequential ADS implementation architecture. In addition, the proposed MMAE ADS scheme may potentially be capable of addressing future demands to fulfill missions that require low-cost low grade gyro products such as fiber optic gyros or Micro-Electro-Mechanical Systems (MEMS) chip based gyros. The ability to calibrate gyro scale factor errors and address its stability subject to thermal or rate variations, especially for the asymmetric components, is clearly critical to the possible deployment of these MEMS gyros for future space missions.

2.0 PROBLEM STATEMENT AND RESEARCH MOTIVATION

A traditional 6-state attitude determination filter contains three attitude error and three gyro bias error states, which is robust during low rate operation but cannot correct for gyro scale factor and misalignment error effects during high rate operation. Under such operating conditions, gyro scale factor and misalignment errors strongly degrade the 6-state filter performance. We use a multi rate profile consisting of various rate magnitudes nominally required during imaging mode to illustrate the existence of a multi-mode operating condition for which a single filter based ADS implementation scheme can not provide adequate attitude knowledge performance. We present the story of this high rate operation impact to the traditional 6 state EKF performance, with and without scale factor (SF) error effects, to show that a higher EKF state dimension vector is definitely needed to restore or maintain a precision attitude estimation capability.

Figures 1 and 2 present the simulation results of a 6 state EKF performance at high rate with the SF errors being turned off or unaccounted for in the gyro model. This case shows that naïve simulation and analysis predict "deceptively" good performance for a 6 state EKF under high rate operating conditions. Figures 3 and 4 present the performance of the 6 state EKF under the same rate profile when we add SF errors to our own gyro model. The impact of SF errors due to high rate operating condition clearly shows in the gyro bias error estimate due to the mixing of SF errors spilled into the bias error, and thus degrading the attitude error estimation accuracy.

The performance impact (loss of precision attitude estimation accuracy shown in Figures 3 and 4) at high rate operating condition to the 6 state EKF due to the SF error effect, and of course the misalignment errors clearly justifies for the need of a higher dimension EKF to estimate the gyro's other error sources and compensate for them at the gyro measurement correction. This leads to the development of a 15 state EKF which is described in the subsequent section.

3.0 DEVELOPMENT OF A 15 STATE EXTENDED KALMAN FILTER (EKF)

3.1 QUATERNION PARAMETERIZATION AND GYRO MODEL

For spacecraft attitude estimation, the quaternion has been the most widely used attitude parameterization [1]. The quaternion is given by a four-dimensional vector, defined as

$$\mathbf{q} = \begin{bmatrix} \mathbf{q}_{13} \\ q_4 \end{bmatrix} \tag{1}$$

with $\mathbf{q}_{13} \equiv \begin{bmatrix} q_1 & q_2 & q_3 \end{bmatrix}^T = \mathbf{d}\sin(\vartheta/2)$ and $q_4 = \cos(\vartheta/2)$, where $\mathbf{d}$ is the unit Euler axis and ϑ is the rotation angle. Because a four-dimensional vector is used to describe three dimensions, the quaternion components cannot be independent of each other. The quaternion satisfies a single constraint given by $\mathbf{q}^T\mathbf{q} = 1$. The attitude matrix is related to the quaternion by

$$A(\mathbf{q}) = \Xi^T(\mathbf{q})\Psi(\mathbf{q}) \tag{2}$$

with

$$\Xi(\mathbf{q}) \equiv \begin{bmatrix} q_4 I_{3\times3} + [\mathbf{q}_{13}\times] \\ -\mathbf{q}_{13}^T \end{bmatrix} \tag{3a}$$

$$\Psi(\mathbf{q}) \equiv \begin{bmatrix} q_4 I_{3\times3} - [\mathbf{q}_{13}\times] \\ -\mathbf{q}_{13}^T \end{bmatrix} \tag{3b}$$

where $I_{3\times3}$ is a 3×3 identity matrix and $[\mathbf{q}_{13}\times]$ is the cross product matrix, defined by

$$[\mathbf{q}_{13}\times] \equiv \begin{bmatrix} 0 & -q_3 & q_2 \\ q_3 & 0 & -q_1 \\ -q_2 & q_1 & 0 \end{bmatrix} \tag{4}$$

For small angles the vector part of the quaternion is approximately equal to half angles [2].

The quaternion kinematics equation is given by

$$\dot{\mathbf{q}} = \frac{1}{2}\Xi(\mathbf{q})\boldsymbol{\omega} \tag{5}$$

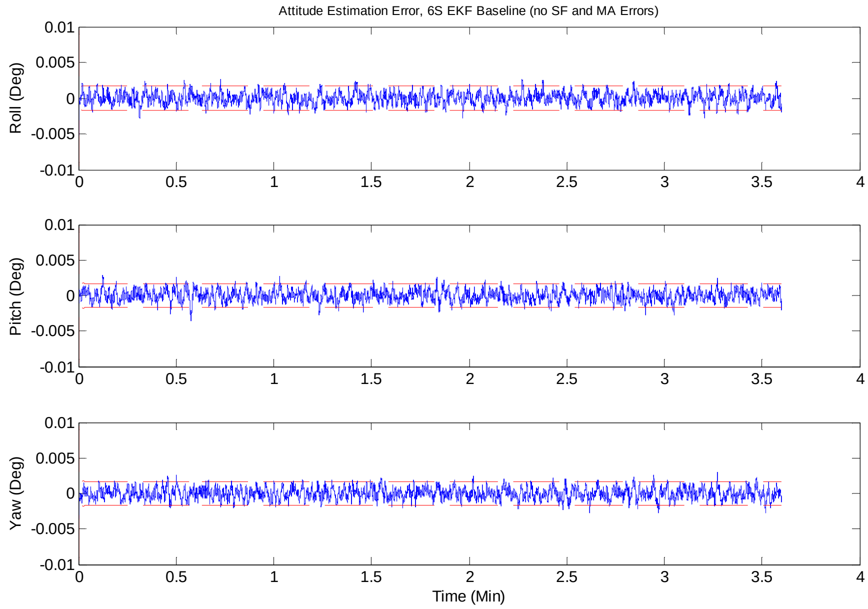

Figure 1: Attitude Estimation Accuracy, 1sig=[2.8   2.9 3.0] arcsecs – (At high rate condition with low fidelity gyro model, attitude estimation performance accuracy looks deceptively good!)

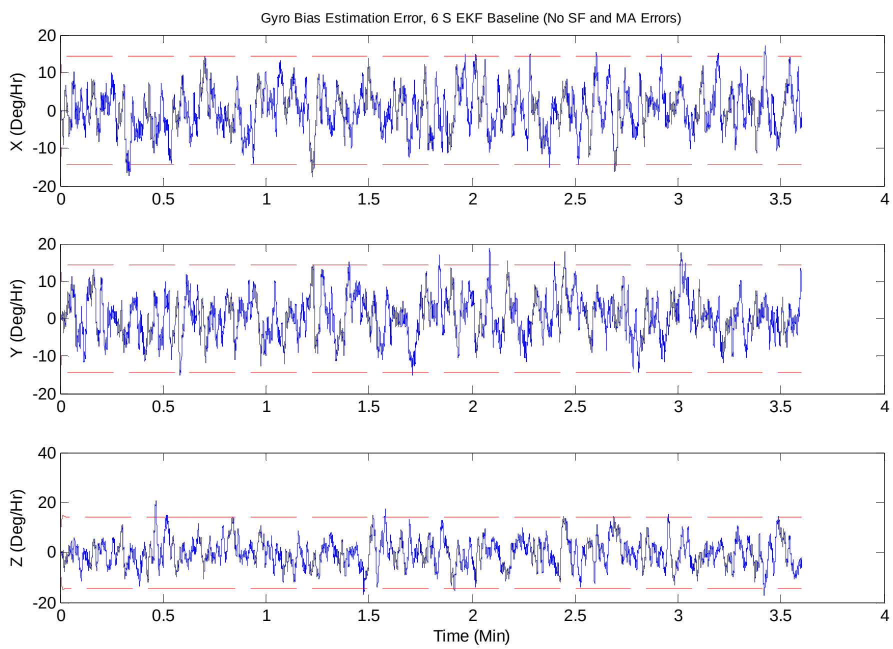

Figure 2: Gyro Bias Estimate (No SF Modeling in Gyro Model)

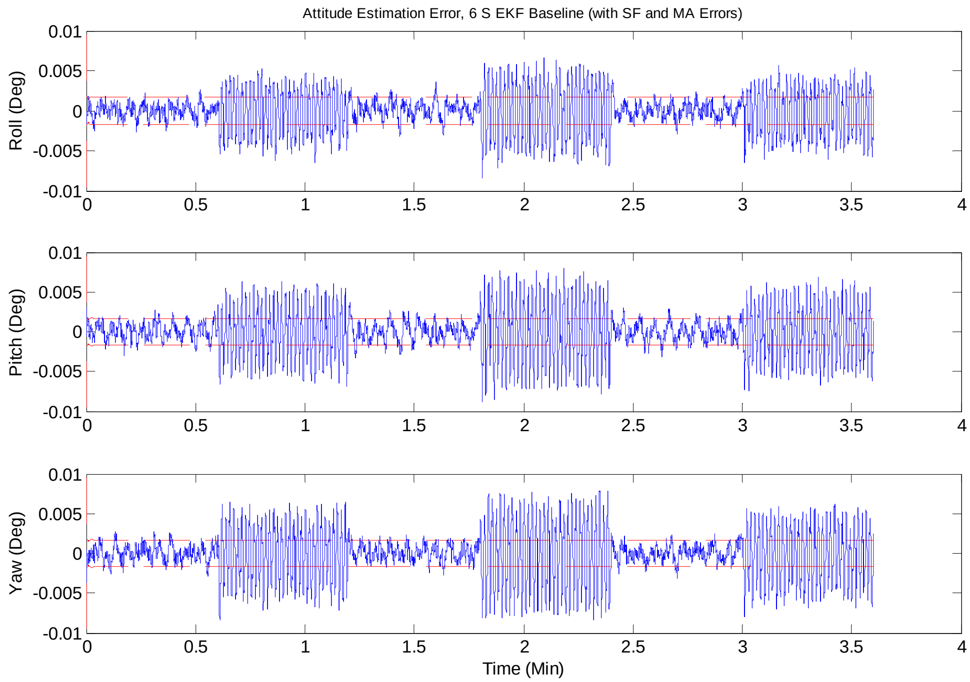

Figure 3: Attitude Estimation Accuracy, 1sig=[8.4 8.9 10.0] arcsecs – (With the Scale Factor (SF) & Mis-Alignment (MA) errors Accounted in Gyro Model, resulting in a loss of ~ [5.2 6.0 7.0] arcsec accuracy in three axes)

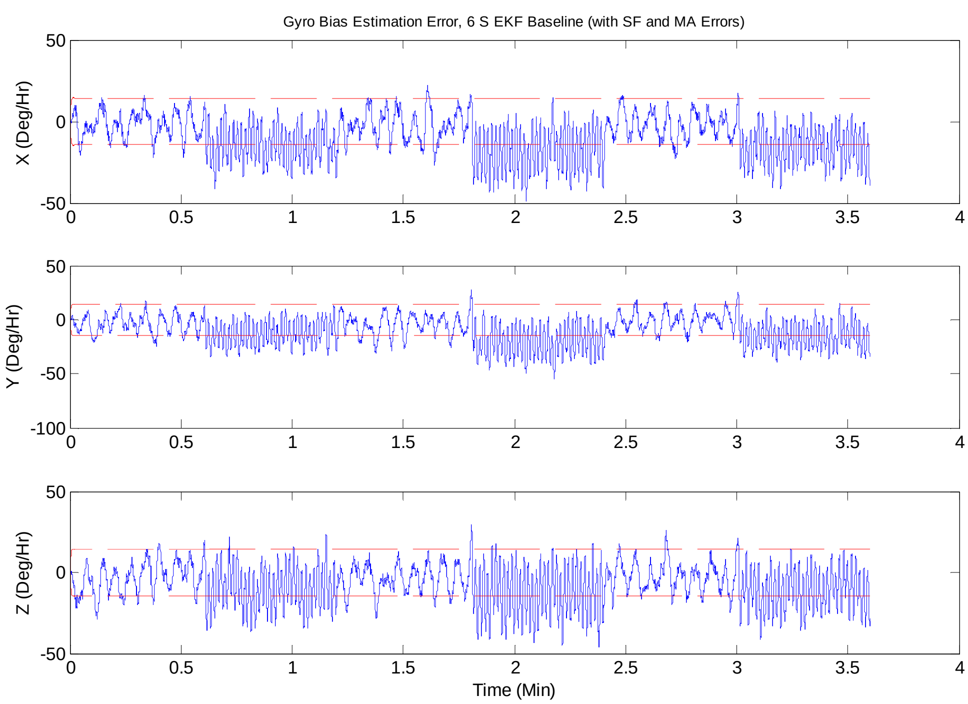

Figure 4: Gyro Bias Estimate Subject to SF Error Modeling (With SF Error turned on, it now affects the gyro bias estimate accuracy in the roll and pitch axes!)

where $\boldsymbol{\omega}$ is the three-component angular rate vector. A major advantage of using the quaternion is that the kinematics equation is linear in the quaternion and is also free of singularities. Another advantage of the quaternion is that successive rotations can be accomplished using quaternion multiplication. Here the convention of [2] is adopted, where the quaternions are multiplied in the same order as the attitude matrix multiplication, in contrast to the usual convention established by Hamilton. A successive rotation is written using $A(\mathbf{q}')A(\mathbf{q}) = A(\mathbf{q}'\otimes\mathbf{q})$. The composition of the quaternions is bilinear, with

$$\mathbf{q}'\otimes\mathbf{q} = \begin{bmatrix}\Psi(\mathbf{q}') & \mathbf{q}'\end{bmatrix}\mathbf{q} = \begin{bmatrix}\Xi(\mathbf{q}) & \mathbf{q}\end{bmatrix}\mathbf{q}' \tag{6}$$

Also, the inverse quaternion is given by $\mathbf{q}^{-1} \equiv \begin{bmatrix}-\mathbf{q}_{13}^T & q_4\end{bmatrix}^T$, with $A(\mathbf{q}^{-1}) = A^T(\mathbf{q})$. Note that $\mathbf{q}\otimes\mathbf{q}^{-1} = \begin{bmatrix}0 & 0 & 0 & 1\end{bmatrix}^T$, which is the identity quaternion.

A common sensor that measures the angular rate is a rate integrating gyro. For this sensor, a widely used three-axis continuous-time model is given by

$$\begin{aligned}
\tilde{\boldsymbol{\omega}} &= (I_{3\times3} + S)\boldsymbol{\omega} + \mathbf{b} + \boldsymbol{\eta}_v\\
\dot{\mathbf{b}} &= \boldsymbol{\eta}_u\\
\dot{\mathbf{s}} &= \boldsymbol{\eta}_s\\
\dot{\mathbf{k}}_U &= \boldsymbol{\eta}_U\\
\dot{\mathbf{k}}_L &= \boldsymbol{\eta}_L\\
S &\equiv \begin{bmatrix} s_1 & k_{U1} & k_{U2}\\ k_{L1} & s_2 & k_{U3}\\ k_{L2} & k_{L3} & s_3\end{bmatrix}
\end{aligned} \tag{7}$$

where $\tilde{\boldsymbol{\omega}}$ is the measured rate, $\mathbf{b}$ is the drift, S is a matrix of scale factors $\mathbf{s}$ and misalignments $\mathbf{k}_U$ and $\mathbf{k}_L$, and $\boldsymbol{\eta}_v$ (i.e., angular random walk, ARW), $\boldsymbol{\eta}_u$ (i.e., rate random walk, RRW) and $\boldsymbol{\eta}_s$, $\boldsymbol{\eta}_U$ and $\boldsymbol{\eta}_L$ are independent zero-mean Gaussian white-noise processes with

$$\begin{aligned}
E\left\{\boldsymbol{\eta}_v(t)\boldsymbol{\eta}_v^T(\tau)\right\} &= \sigma_v^2\delta(t-\tau)I_{3\times3}\\
E\left\{\boldsymbol{\eta}_u(t)\boldsymbol{\eta}_u^T(\tau)\right\} &= \sigma_u^2\delta(t-\tau)I_{3\times3}\\
E\left\{\boldsymbol{\eta}_s(t)\boldsymbol{\eta}_s^T(\tau)\right\} &= \sigma_s^2\delta(t-\tau)I_{3\times3}\\
E\left\{\boldsymbol{\eta}_U(t)\boldsymbol{\eta}_U^T(\tau)\right\} &= \sigma_U^2\delta(t-\tau)I_{3\times3}\\
E\left\{\boldsymbol{\eta}_L(t)\boldsymbol{\eta}_L^T(\tau)\right\} &= \sigma_L^2\delta(t-\tau)I_{3\times3}
\end{aligned} \tag{8}$$

where E{ } denotes expectation and $\delta(t-\tau)$ is the Dirac-delta function. A discrete-time version of Eq. (7) is given in [3].

3.2 KALMAN FILTERING FOR ATTITUDE ESTIMATION

This section provides a review of the equations involved for spacecraft attitude estimation using the Kalman filter. The measurements are assumed to be given for a star tracker determined Kalman filter. To within first-order the quaternion measurements can be modeled by

$$\tilde{\mathbf{q}} = \mathbf{q} + \frac{1}{2}\Xi(\mathbf{q})\mathbf{v} \tag{9}$$

where $\tilde{\mathbf{q}}$ is the measurement quaternion and $\mathbf{v}$ is a zero-mean Gaussian process with covariance R. Note that $\mathbf{v}$ is not a stationary process and R is determined from the attitude error-covariance of the attitude determination process [4]. Also, to within first-order the quaternion normalization constraint is maintained with this measurement model. A summary of the extended Kalman filter (EKF) for attitude estimation, including gyro drifts and scale factors, is shown in Table 1. All symbols and characters with a hat over them signify estimates. The variables P_k^+ and P_k^- denote the updated and propagated error-covariance at time t_k, respectively; K_k is the Kalman gain; the first three components of $\Delta\hat{\mathbf{x}}$, denoted by $\boldsymbol{\delta}\hat{\boldsymbol{\alpha}}$, are the small-attitude error estimates, and the vector $\hat{\mathbf{s}}$ denotes the diagonal elements of the estimate scale factor matrix, $\hat{S}$. Note that the propagated values for the gyro drift and scale factors are given by their previous time values.

We now derive the $F(t)$ and $G(t)$ matrices. Here it is assumed that $(I_{3\times3}+S)^{-1} \approx (I_{3\times3}-S)$, which is valid for small S. A multiplicative error quaternion is used to derive the attitude errors:

$$\boldsymbol{\delta}\mathbf{q} = \mathbf{q}\otimes\hat{\mathbf{q}}^{-1} \approx \begin{bmatrix}0.5\boldsymbol{\delta\alpha}\\ 1\end{bmatrix} \tag{10}$$

where $\boldsymbol{\delta\alpha}$ is the vector of small attitude (roll, pitch and yaw) attitude errors. The error-kinematics follow [1]

$$\boldsymbol{\delta}\dot{\boldsymbol{\alpha}} = -\left[\hat{\boldsymbol{\omega}}\times\right]\boldsymbol{\delta\alpha} + \boldsymbol{\delta\omega} \tag{11}$$

where $\boldsymbol{\delta\omega} \equiv \boldsymbol{\omega} - \hat{\boldsymbol{\omega}}$. From Eq. (7) we have

$$\begin{aligned}
\boldsymbol{\omega} &= (I_{3\times3}-S)\tilde{\boldsymbol{\omega}} - (I_{3\times3}-S)\mathbf{b} - (I_{3\times3}-S)\boldsymbol{\eta}_v\\
\hat{\boldsymbol{\omega}} &= (I_{3\times3}-\hat{S})\tilde{\boldsymbol{\omega}} - (I_{3\times3}-\hat{S})\hat{\mathbf{b}}
\end{aligned} \tag{12}$$

Then $\boldsymbol{\delta\omega}$ is given by

$$\begin{aligned}
\boldsymbol{\delta\omega} &= -\Delta S\,\tilde{\boldsymbol{\omega}} - \Delta\mathbf{b} + (\Delta S + \hat{S})(\Delta\mathbf{b} + \hat{\mathbf{b}}) - \hat{S}\,\hat{\mathbf{b}}\\
&\quad -(I_{3\times3} - \hat{S} - \Delta S)\boldsymbol{\eta}_v
\end{aligned} \tag{13}$$

where $\Delta S \equiv S - \hat{S}$ and $\Delta\mathbf{b} \equiv \mathbf{b} - \hat{\mathbf{b}}$. Ignoring second-order terms leads to

TABLE 1: EKF FOR ATTITUDE ESTIMATION

Initialize	$\hat{\mathbf{q}}(t_0)=\hat{\mathbf{q}}_0,\quad \hat{\mathbf{b}}(t_0)=\hat{\mathbf{b}}_0,\quad \hat{\mathbf{s}}(t_0)=\hat{\mathbf{s}}_0$ $\hat{\mathbf{k}}_U(t_0)=\hat{\mathbf{k}}_{U0},\quad \hat{\mathbf{k}}_L(t_0)=\hat{\mathbf{k}}_{L0}$ $P(t_0)=P_0$
Compute Gain	$K_k=P_k^- H^T\left(H\,P_k^- H^T+R_k\right)^{-1}$ $H=\left[I_{3\times3}\quad 0_{3\times3}\quad 0_{3\times3}\quad 0_{3\times3}\quad 0_{3\times3}\right]$
Update	$P_k^+=\left(I_{15\times15}-K_k H\right)P_k^-$ $\Delta\hat{\mathbf{x}}_k^+=2K_k\,\Xi^T\left(\hat{\mathbf{q}}_k^-\right)\tilde{\mathbf{q}}_k$ $\Delta\hat{\mathbf{x}}_k^+\equiv\left[\boldsymbol{\delta}\hat{\boldsymbol{\alpha}}_k^{+T}\quad \Delta\hat{\mathbf{b}}_k^{+T}\quad \Delta\hat{\mathbf{s}}_k^{+T}\quad \Delta\hat{\mathbf{k}}_{Uk}^{+T}\quad \Delta\hat{\mathbf{k}}_{Lk}^{+T}\right]^{TT}$ $\hat{\mathbf{q}}_k^+=\hat{\mathbf{q}}_k^-+\frac{1}{2}\Xi\left(\hat{\mathbf{q}}_k^-\right)\boldsymbol{\delta}\hat{\boldsymbol{\alpha}}_k^{+T}$, re-normalize $\hat{\mathbf{b}}_k^+=\hat{\mathbf{b}}_k^-+\Delta\hat{\mathbf{b}}_k^+$ $\hat{\mathbf{s}}_k^+=\hat{\mathbf{s}}_k^-+\Delta\hat{\mathbf{s}}_k^+$ $\hat{\mathbf{k}}_{Uk}^+=\hat{\mathbf{k}}_{Uk}^-+\Delta\hat{\mathbf{k}}_{Uk}^+$ $\hat{\mathbf{k}}_{Lk}^+=\hat{\mathbf{k}}_{Lk}^-+\Delta\hat{\mathbf{k}}_{Lk}^+$
Propagate	$\hat{\boldsymbol{\omega}}(t)=\left[I_{3\times3}-\hat{S}(t)\right]\left[\tilde{\boldsymbol{\omega}}(t)-\hat{\mathbf{b}}(t)\right]$ $\dot{\hat{\mathbf{q}}}=\frac{1}{2}\Xi\left[\hat{\mathbf{q}}(t)\right]\hat{\boldsymbol{\omega}}(t)$ $\dot{\hat{\mathbf{b}}}(t)=\mathbf{0}$ $\dot{\hat{\mathbf{s}}}(t)=\mathbf{0}$ $\dot{\hat{\mathbf{k}}}_U=\mathbf{0}$ $\dot{\hat{\mathbf{k}}}_L=\mathbf{0}$ $\dot{P}(t)=F(t)P(t)+P(t)F^T(t)+G(t)Q(t)G^T(t)$

$$
\begin{aligned}
\boldsymbol{\delta\omega}&=\left(I_{3\times3}-\hat{S}\right)\Delta\mathbf{b}-\mathrm{diag}\left(\tilde{\boldsymbol{\omega}}-\hat{\mathbf{b}}\right)\Delta\mathbf{s}\\
&\quad-\hat{U}\,\Delta\mathbf{k}_U-\hat{L}\,\Delta\mathbf{k}_L-\left(I_{3\times3}-\hat{S}\right)\boldsymbol{\eta}_v\\
\hat{U}&=\begin{bmatrix}\tilde{\omega}_2-\hat{b}_2 & \tilde{\omega}_3-\hat{b}_3 & 0\\ 0 & 0 & \tilde{\omega}_3-\hat{b}_3\\ 0 & 0 & 0\end{bmatrix}\\
\hat{L}&=\begin{bmatrix}0 & 0 & 0\\ \tilde{\omega}_1-\hat{b}_1 & 0 & 0\\ 0 & \tilde{\omega}_1-\hat{b}_1 & \tilde{\omega}_2-\hat{b}_2\end{bmatrix}
\end{aligned}
\tag{14}
$$

where diag denotes a diagonal matrix, $\Delta\mathbf{s}$ is a vector of the diagonal elements of ΔS, and $\Delta\mathbf{k}_U$ and $\Delta\mathbf{k}_L$ correspond to the upper and lower off-diagonal elements of ΔS. Hence, the matrices $F(t)$, $G(t)$ and $Q(t)$ are given by

$$F=\begin{bmatrix} -[\hat{\boldsymbol{\omega}}\times] & -\left(I_{3\times3}-\hat{S}\right) & \mathrm{diag}\left(\tilde{\boldsymbol{\omega}}-\hat{\mathbf{b}}\right) & \hat{U} & \hat{L} \\ 0_{3\times3} & 0_{3\times3} & 0_{3\times3} & 0_{3\times3} & 0_{3\times3} \\ 0_{3\times3} & 0_{3\times3} & 0_{3\times3} & 0_{3\times3} & 0_{3\times3} \\ 0_{3\times3} & 0_{3\times3} & 0_{3\times3} & 0_{3\times3} & 0_{3\times3} \\ 0_{3\times3} & 0_{3\times3} & 0_{3\times3} & 0_{3\times3} & 0_{3\times3} \end{bmatrix}$$

$$G=\begin{bmatrix} -\left(I_{3\times3}-\hat{S}\right) & 0_{3\times3} & 0_{3\times3} & 0_{3\times3} & 0_{3\times3} \\ 0_{3\times3} & I_{3\times3} & 0_{3\times3} & 0_{3\times3} & 0_{3\times3} \\ 0_{3\times3} & 0_{3\times3} & I_{3\times3} & 0_{3\times3} & 0_{3\times3} \\ 0_{3\times3} & 0_{3\times3} & 0_{3\times3} & I_{3\times3} & 0_{3\times3} \\ 0_{3\times3} & 0_{3\times3} & 0_{3\times3} & 0_{3\times3} & I_{3\times3} \end{bmatrix}$$

$$Q=\begin{bmatrix} \sigma_v^2 I_{3\times3} & 0_{3\times3} & 0_{3\times3} & 0_{3\times3} & 0_{3\times3} \\ 0_{3\times3} & \sigma_u^2 I_{3\times3} & 0_{3\times3} & 0_{3\times3} & 0_{3\times3} \\ 0_{3\times3} & 0_{3\times3} & \sigma_s^2 I_{3\times3} & 0_{3\times3} & 0_{3\times3} \\ 0_{3\times3} & 0_{3\times3} & 0_{3\times3} & \sigma_U^2 I_{3\times3} & 0_{3\times3} \\ 0_{3\times3} & 0_{3\times3} & 0_{3\times3} & 0_{3\times3} & \sigma_L^2 I_{3\times3} \end{bmatrix} \tag{15}$$

A discrete-time propagation of the quaternion and error-covariance is possible (see [5] for details). The discrete-time covariance propagation is given by

$$P_k^- = \Phi_k P_k^+ \Phi_k^T + Q_k \tag{16}$$

where Φ_k and Q_k are discrete-time state transition and process-noise covariance matrices, respectively. For small sampling intervals the discrete process noise matrix is well approximated by (also see [8])

$$\Phi_k \approx I_{15\times15} + \Delta t\, F(t) + \frac{1}{2}\Delta t^2\, F^2(t)$$

$$Q_k \approx \begin{bmatrix} \left(\sigma_v^2+\frac{1}{3}\sigma_u^2\Delta t^2\right)\Delta t\, I_{3\times3}+\frac{1}{3}\sigma_s^2\Delta t^3\Omega^2(\hat{\boldsymbol{\omega}}_k) & -\frac{1}{2}\sigma_u^2\Delta t^2 I_{3\times3} & -\frac{1}{2}\sigma_s^2\Delta t^2\Omega^2(\hat{\boldsymbol{\omega}}_k) & \frac{1}{2}\sigma_U^2\Delta t^2\hat{U} & \frac{1}{2}\sigma_L^2\Delta t^2\hat{L} \\ -\frac{1}{2}\sigma_u^2\Delta t^2 I_{3\times3} & \sigma_u^2\Delta t^2 I_{3\times3} & 0_{3\times3} & 0_{3\times3} & 0_{3\times3} \\ -\frac{1}{2}\sigma_s^2\Delta t^2\Omega^2(\hat{\boldsymbol{\omega}}_k) & 0_{3\times3} & \sigma_v^2\Delta t^2 I_{3\times3} & 0_{3\times3} & 0_{3\times3} \\ \frac{1}{2}\sigma_U^2\Delta t^2\hat{U}^T & 0_{3\times3} & 0_{3\times3} & \sigma_U^2\Delta t^2 I_{3\times3} & 0_{3\times3} \\ \frac{1}{2}\sigma_L^2\Delta t^2\hat{L}^T & 0_{3\times3} & 0_{3\times3} & 0_{3\times3} & \sigma_L^2\Delta t^2 I_{3\times3} \end{bmatrix} \tag{17}$$

where Δt is the sampling interval and $\Omega(\hat{\boldsymbol{\omega}}_k)$ is a diagonal matrix made up of the elements of the estimate rate.

4.0 MULTIPLE-MODEL ADAPTIVE ESTIMATION

4.1 MMAE FORMULATION

In this section a review of MMAE is shown. More details can be found in [6]. Multiple-model adaptive estimation is a recursive estimator that uses a bank of filters that depend on some unknown parameters. In our case these parameters are the process noise covariance, denoted by the vector $\mathbf{p}$, which is assumed to be constant (at least throughout the interval of adaptation). Note that we do not necessarily need to make the stationary assumption for the state and/or output processes though, i.e. time varying state and output matrices can be used. A set of distributed elements is generated from some known probability density function (pdf) of $\mathbf{p}$, denoted by $p(\mathbf{p})$, to give $\left\{\mathbf{p}^{(\ell)};\ell=1,\ldots,M\right\}$.

The goal of the estimation process is to determine the conditional pdf of the ℓ^{th} element of $\mathbf{p}^{(\ell)}$ given the current-time measurement $\tilde{\mathbf{y}}_k$. Application of Bayes rule yields

$$p\left(\mathbf{p}^{(\ell)}\,|\,\tilde{\mathbf{Y}}_k\right)=\frac{p\left(\tilde{\mathbf{Y}}_k\,|\,\mathbf{p}^{(\ell)}\right)p\left(\mathbf{p}^{(\ell)}\right)}{\sum_{j=1}^{M}p\left(\tilde{\mathbf{Y}}_k\,|\,\mathbf{p}^{(j)}\right)p\left(\mathbf{p}^{(j)}\right)} \tag{18}$$

where $\tilde{\mathbf{Y}}_k$ denotes the sequence $\{\tilde{\mathbf{y}}_0,\tilde{\mathbf{y}}_1,\ldots,\tilde{\mathbf{y}}_k\}$. The *a posteriori* probabilities can be computed through

$$p\left(\mathbf{p}^{(\ell)} \mid \tilde{\mathbf{Y}}_k\right) = \frac{p\left(\tilde{\mathbf{y}}_k, \mathbf{p}^{(\ell)} \mid \tilde{\mathbf{Y}}_{k-1}\right)}{p\left(\tilde{\mathbf{y}}_k \mid \tilde{\mathbf{Y}}_{k-1}\right)} = \frac{p\left(\tilde{\mathbf{y}}_k \mid \hat{\mathbf{x}}_k^{-(\ell)}\right) p\left(\mathbf{p}^{(\ell)} \mid \tilde{\mathbf{Y}}_{k-1}\right)}{\sum_{j=1}^{M} p\left(\tilde{\mathbf{y}}_k \mid \hat{\mathbf{x}}_k^{-(j)}\right) p\left(\mathbf{p}^{(j)} \mid \tilde{\mathbf{Y}}_{k-1}\right)} \tag{19}$$

where $\hat{\mathbf{x}}_k^{-(\ell)}$ denotes the propagated state estimate of the ℓ th Kalman filter. Note that the denominator of Eq. (19) is just a normalizing factor to ensure that $p\left(\mathbf{p}^{(\ell)} \mid \tilde{\mathbf{Y}}_k\right)$ is a pdf. The recursion formula can now be cast into a set of defined weights $\varpi_k^{(\ell)}$

$$\begin{aligned} \varpi_k^{(\ell)} &= \varpi_{k-1}^{(\ell)}\, p\left(\tilde{\mathbf{y}}_k \mid \hat{\mathbf{x}}_k^{-(\ell)}\right) \\ \varpi_k^{(\ell)} &\leftarrow \frac{\varpi_k^{(\ell)}}{\sum_{j=1}^{M} \varpi_k^{(\ell)}} \end{aligned} \tag{20}$$

where $\varpi_k^{(\ell)} \equiv p\left(\mathbf{p}^{(\ell)} \mid \tilde{\mathbf{Y}}_{k-1}\right)$. The weights are initialized to $\varpi_0^{(\ell)} = 1/M$ for $\ell = 1, 2, \ldots, M$. Note that $p\left(\tilde{\mathbf{y}}_k \mid \hat{\mathbf{x}}_k^{-(\ell)}\right)$ denotes the likelihood function.

The conditional mean estimate is the weighted sum of the parallel filter estimates

$$\hat{\mathbf{x}}_k^{-} = \sum_{j=1}^{M} \varpi_k^{(j)} \hat{\mathbf{x}}_k^{-(j)} \tag{21}$$

Also, the error covariance of the state estimate can be computed using

$$P_k^{-} = \sum_{j=1}^{M} \varpi_k^{(j)} \left(\hat{\mathbf{x}}_k^{-(j)} - \hat{\mathbf{x}}_k^{-}\right)\left(\hat{\mathbf{x}}_k^{-(j)} - \hat{\mathbf{x}}_k^{-}\right)^T \tag{22}$$

The specific estimate for $\mathbf{p}$ at time t_k, denoted by $\hat{\mathbf{p}}_k$, and error covariance, denoted by Z_k, are given by

$$\hat{\mathbf{p}}_k = \sum_{j=1}^{M} \varpi_k^{(j)} \mathbf{p}^{(j)} \tag{23a}$$

$$Z_k = \sum_{j=1}^{M} \varpi_k^{(j)} \left(\mathbf{p}^{(j)} - \hat{\mathbf{p}}_k\right)\left(\mathbf{p}^{(j)} - \hat{\mathbf{p}}_k\right)^T \tag{23b}$$

Equation (23b) can be used to define 3σ bounds on the estimate $\hat{\mathbf{p}}_k$.

4.2 ATTITUDE LIKELIHOOD FUNCTION

This section derives the likelihood function for the MMAE algorithm using quaternion measurements. From Table 1, the measurement residual is defined to be (ignoring the propagated notation for $\hat{\mathbf{q}}$)

$$\mathbf{e} \equiv 2\Xi^T(\hat{\mathbf{q}})\tilde{\mathbf{q}} \tag{24}$$

which is derived from the vector part of $\tilde{\mathbf{q}} \otimes \hat{\mathbf{q}}^{-1}$ (the factor of 2 is used so that $\mathbf{e}$ represents half-angle residuals). Using Eq. (9) and $\hat{\mathbf{q}} = \mathbf{q} + \frac{1}{2}\Xi^T(\mathbf{q})\boldsymbol{\delta\alpha}$ in Eq. (24) gives

$$\mathbf{e} = 2\left[\Xi^T(\mathbf{q}) + \frac{1}{2}\Xi^T\left(\Xi(\mathbf{q})\boldsymbol{\delta\alpha}\right)\right]\left[\mathbf{q} + \frac{1}{2}\Xi^T(\mathbf{q})\mathbf{v}\right] \tag{25}$$

Using the identity $\Xi^T\left(\Xi(\mathbf{q})\boldsymbol{\delta\alpha}\right) = -[\boldsymbol{\delta\alpha}\times]\Xi^T(\mathbf{q}) - \boldsymbol{\delta\alpha}\,\mathbf{q}^T$ in Eq. (25) leads to

$$\mathbf{e} = \mathbf{v} - \frac{1}{2}[\boldsymbol{\delta\alpha}\times]\mathbf{v} - \boldsymbol{\delta\alpha} \tag{26}$$

where $\Xi^T(\mathbf{q})\Xi(\mathbf{q}) = I_{3\times3}$, $\Xi^T(\mathbf{q})\mathbf{q} = \mathbf{0}$ and $\mathbf{q}^T\mathbf{q} = 1$ have been used. Therefore, since $\boldsymbol{\delta\alpha}$ and $\mathbf{v}$ are uncorrelated, the covariance of the residual at time t_k, using the propagated values, is given by

$$E\left\{\mathbf{e}_k^{-}\mathbf{e}_k^{-T}\right\} = H\,P_k^{-}H^T + R_k \tag{27}$$

where H is defined in Table 1. Therefore the likelihood function is given by

$$p\left(\tilde{\mathbf{y}}_k \mid \hat{\mathbf{x}}_k^{-(\ell)}\right) = \frac{1}{\left\{\det\left[2\pi\left(H\,P_k^{-(\ell)}H^T + R_k\right)\right]\right\}^{1/2}} \exp\left[-\frac{1}{2}\mathbf{e}_k^{-(\ell)}\left(H\,P_k^{-(\ell)}H^T + R_k\right)^{-1}\mathbf{e}_k^{-(\ell)}\right] \tag{28}$$

which is used to update the weights in the MMAE algorithm.

4.3 AVERAGE QUATERNION

The goal of the MMAE algorithm is to not only update the process noise covariance parameters, but also to provide states estimates. These estimates are given using Eq. (21); however two major problems exist with the quaternion estimates. First there are no guarantees that the averaged quaternion is a normalized vector. Second, it is well known that $\mathbf{q}$ and $-\mathbf{q}$ represent the same rotation, so that the quaternions provide a 2:1 mapping of the rotation group. Thus changing the sign of any quaternion should not change the average, but it is clear that Eq. (21) does not have this property. The observation that we really want to average attitudes rather than quaternions provides a way to avoid both of these flaws. The average quaternion should minimize a weighted sum of the squared Frobenius norm of attitude matrix differences:

$$\hat{\mathbf{q}}_k^- \triangleq \arg\min_{\mathbf{q}\in\mathbb{S}^3} \sum_{j=1}^{M} \varpi_k^{(j)} \left\| A(\mathbf{q}) - A\left(\hat{\mathbf{q}}_k^{-(j)}\right)\right\|_F^2 \tag{29}$$

where $\hat{\mathbf{q}}_k^{-(j)}$ is the estimated quaternion from the j^{th} EKF. Reference [7] provides a solution to this minimization problem. The average quaternion is given as the eigenvector associated with the largest eigenvalue of the following matrix:

$$T = -\sum_{j=1}^{M} \varpi_k^{(j)} \hat{\mathbf{q}}_k^{-(j)} \hat{\mathbf{q}}_k^{-T(j)} \tag{30}$$

Note that the sign of any $\hat{\mathbf{q}}_k^{-(j)}$ does not change the value of the matrix T.

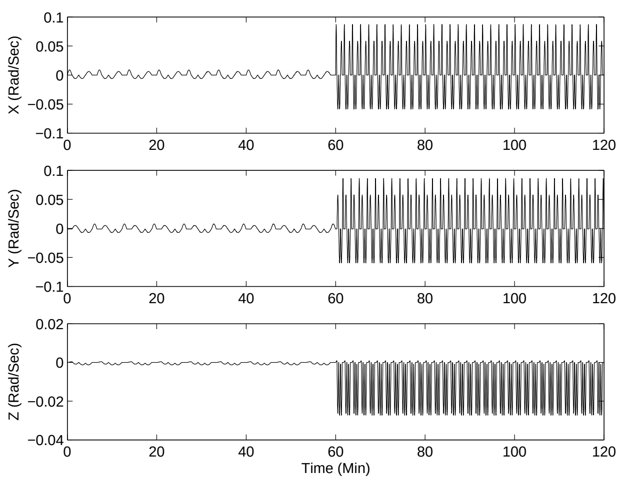

Figure 4: True Body Rates

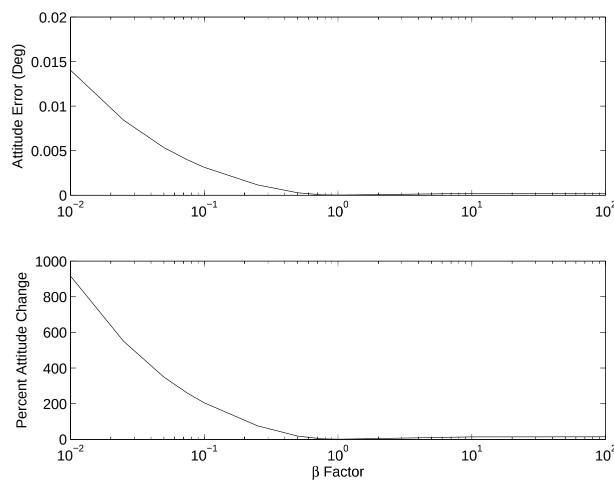

Figure 5: Sensitivity Analysis

4.4 SIMULATION RESULTS OF GYRO NOISE ESTIMATION VIA MMAE SCHEME

This section presents simulation results of the MMAE algorithm to estimate process noise covariance parameters. The true angular rates of the simulated vehicle are shown in Fig. 4. Star tracker measurements are simulated using an isotropic covariance matrix, i.e. $R = \sigma_n^2 I_{3\times3}$, with $\sigma_n = 0.001$ deg. Gyro measurements are simulated with $\sigma_v = 0.1\times(\pi/180)/60\ \text{rad}/\text{sec}^{1/2}$, $\sigma_u = \sqrt{10}\times10^{-10}\ \text{rad}/\text{sec}^{3/2}$, $\sigma_s = 0$ and $S = 500 I_{3\times3}$ PPM. The sampling interval for the star trackers and gyro are 1 sec and 0.01 sec, respectively.

A sensitivity study is performed to assess how the attitude estimation performance is affected by varying gyro noise parameters. Scale factors obviously can greatly affect the overall performance, which is why they are estimated in real time. It is well known that the attitude estimation performance is more affected by σ_v than σ_u. The EKF in Table 1 is executed using σ_u multiplied by some factor β and the norm of the standard deviations of attitude estimates is taken and compared to the results when $\beta = 1$. The attitude errors for varying β are shown in the top plot of Fig. 5. Clearly, the EKF is more sensitive to values of β below 1 than higher than 1. But, using a β greater than one produces an error-covariance that may be conservative, which is undesirable when considering attitude error budgets for the overall estimation process. Significant errors are present when modest variations in σ_v are given. For example when $\beta = 0.3$ the attitude errors are as large as the standard deviation of the noise in the star tracker, which corresponds to a 100% error from the original response, as shown with the bottom plot of Fig. 5. A sensitivity analysis on σ_u has also been performed for the same range of β. These results show that the highest percent error for variations in σ_u is given by only 0.1%, which confirms well-known notions.

Figures 6 and 7 illustrate the effectiveness of the MMAE in estimating the gyro's rate random walk (RRW) and angular random walk (ARW). It is obvious that with the ability to identify the statistics of these noise processes on line, the process noise Q matrix can be adaptively updated in real-time (instead of ad-hoc off-line tuning approach employed in [8]). Therefore, its attitude estimation performance can be further enhanced in a much more efficient manner.

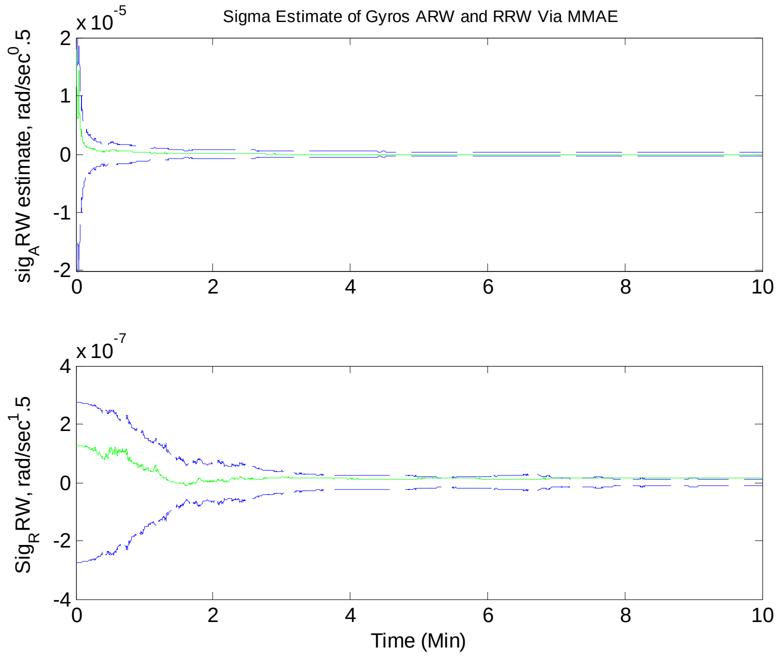

Figure 6: Gyro RRW & ARW Noise Estimation Via MMAE Scheme

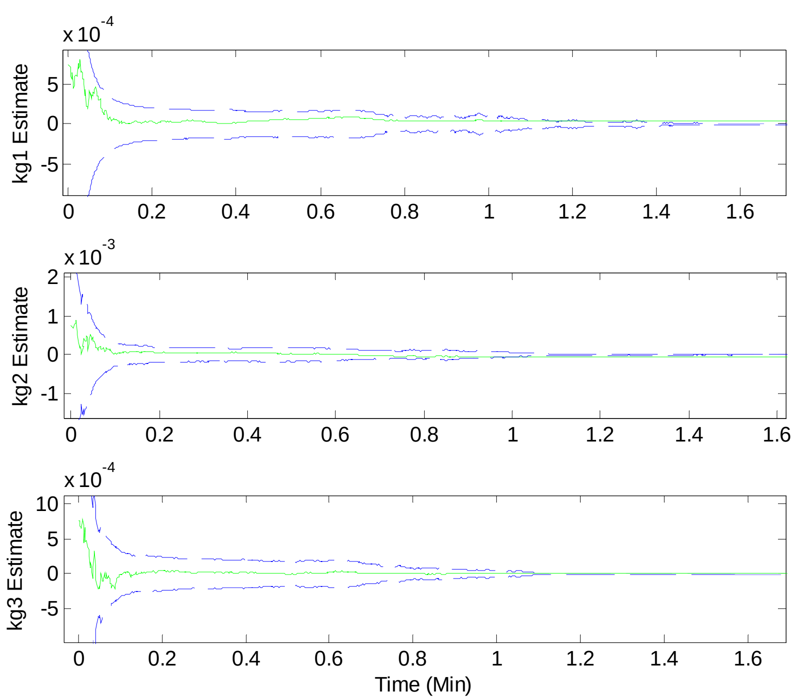

Figure 7: Gyro SF Noise (PPM) Estimation Via MMAE Scheme

4.5 ATTITUDE ESTIMATION PERFORMANCE VIA A SINGLE 15 STATE EKF FILTER

Figures 8 to 12 present a better attitude estimation performance when a 15 state EKF is used under high rate operating condition. It is obvious that the SF and misalignment (MA) error effects have no longer "contaminated" the bias error (see Figures 8 and 9), thus resulting in a performance improvement as compared to the baseline 6 state EKF presented earlier. Nevertheless, the overall performance of the 15 state EKF (depicted in Figures 8 to 12) still does not exhibit an acceptable performance yet. As a result, it leads to the investigation of the multiple EKF models mixing via a linear combination and MMAE approaches which will be discussed within the next two subsections.

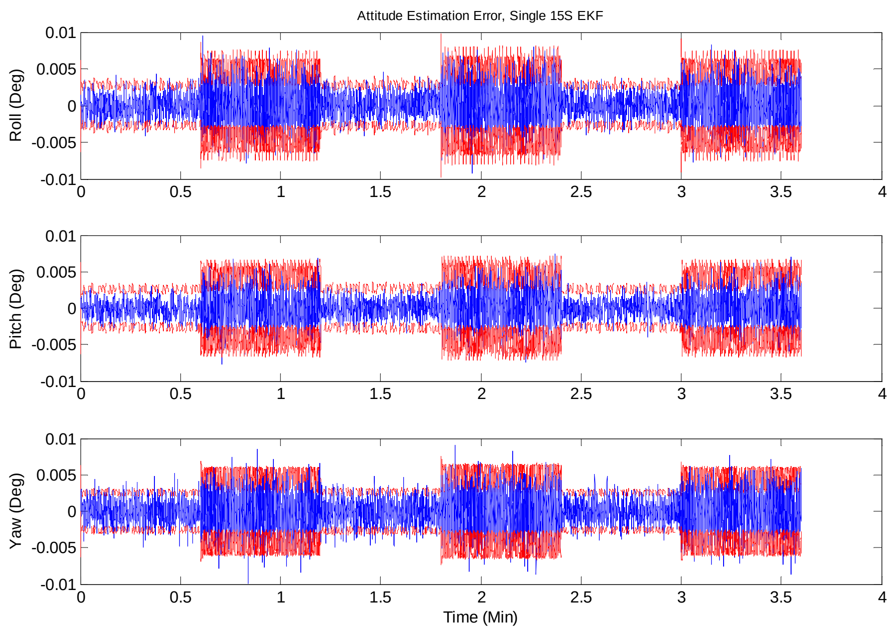

Figure 8: Attitude Estimation Performance of a 15 State EKF
(1sig=[5.9 4.9 6.2] arcsecs, an improved attitude performance over the 6 state EKF presented in Figure 3 but still reflecting poor performance during high rate periods, *especially in the yaw axis***)**

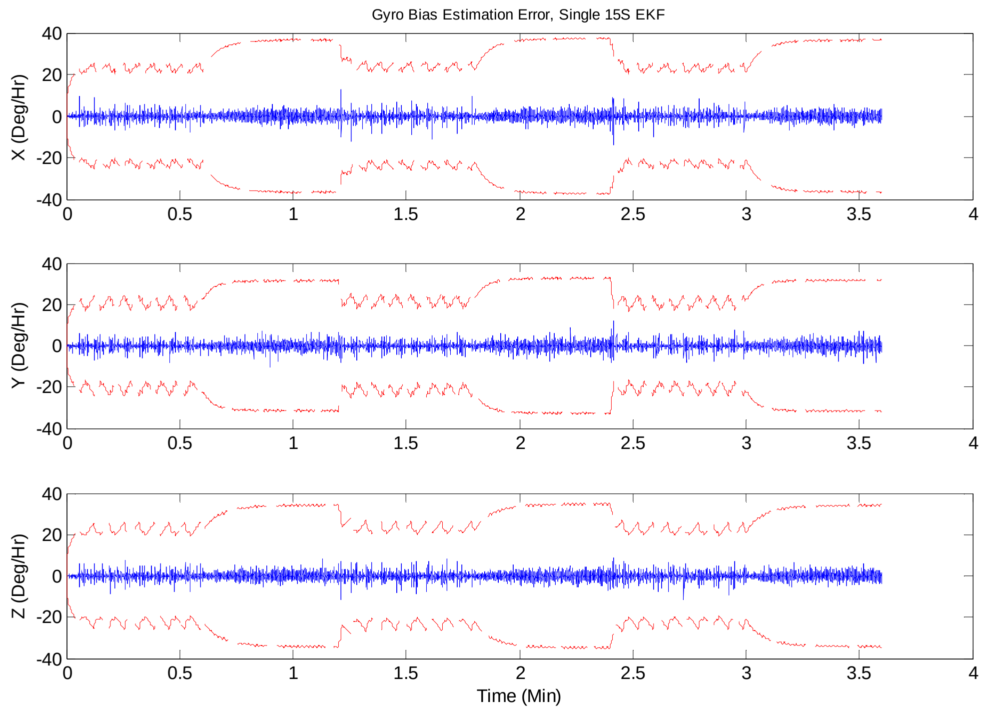

Figure 9: Gyro Bias Estimation Performance of a 15 State EKF

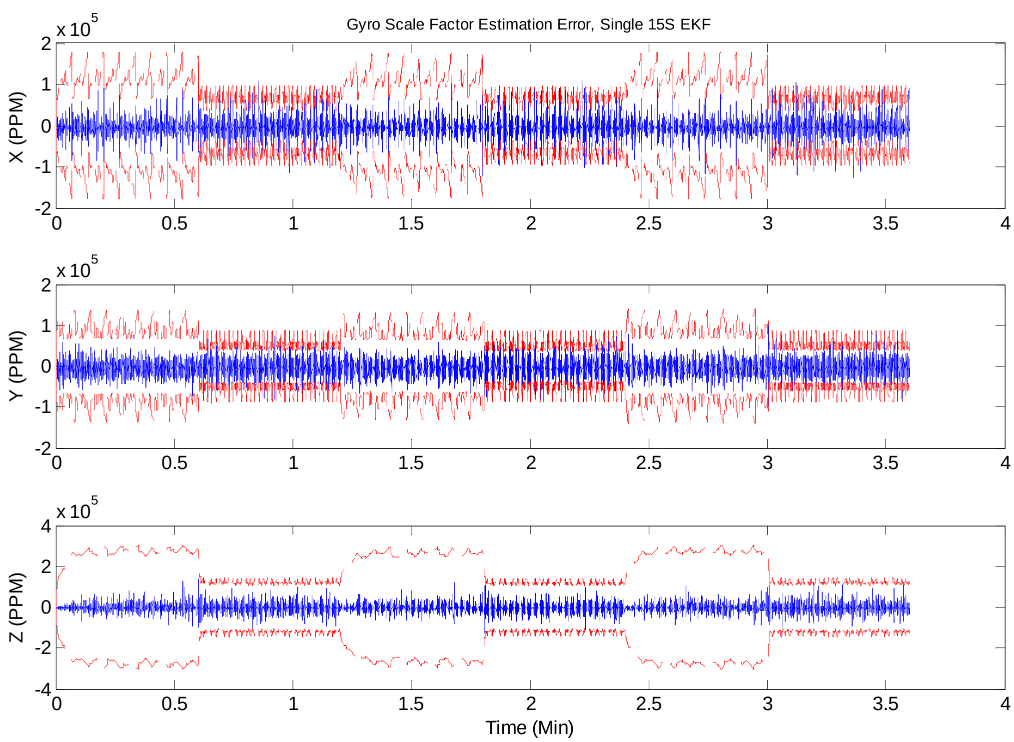

Figure 10: Scale Factor Estimation Performance of a 15 State EKF

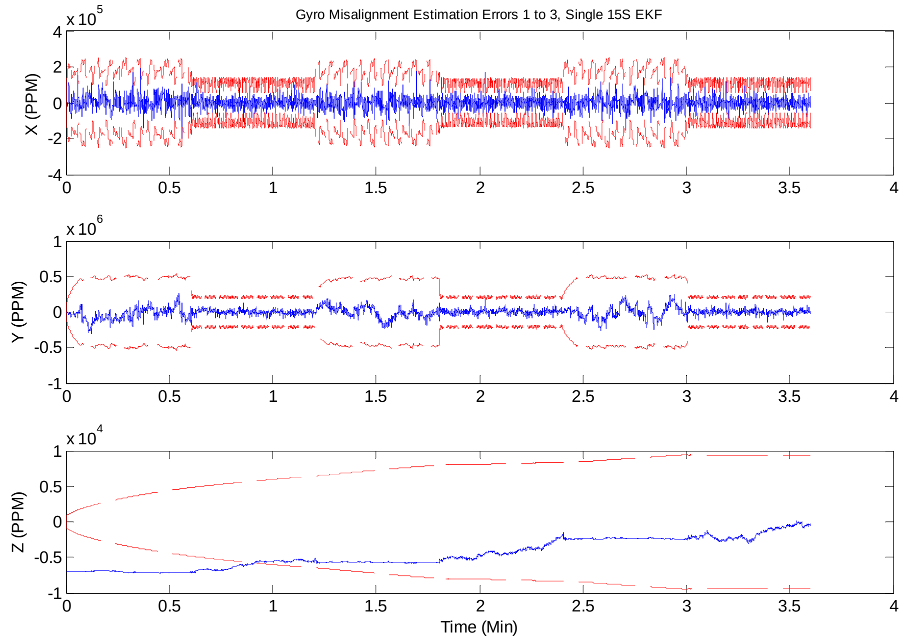

Figure 11: Upper Misalignment (MA) Error Estimation of a 15 State EKF (poor performance in estimating the 3rd upper misalignment error for the first two minutes)

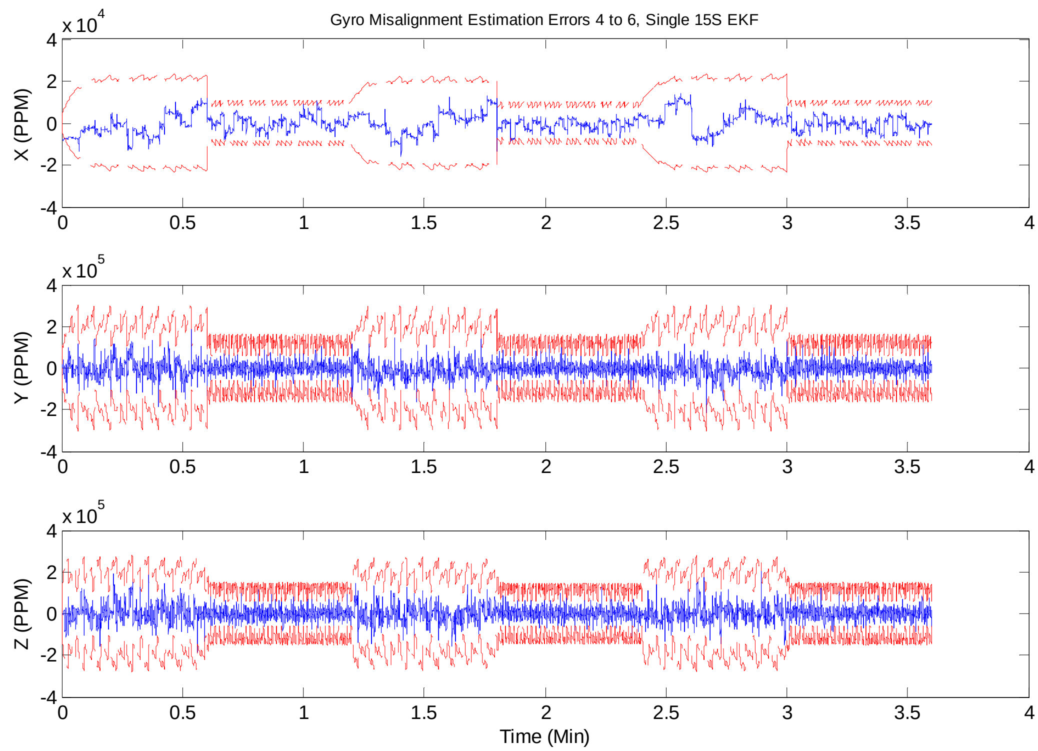

Figure 12: Lower MA Error Estimation of a 15 State EKF

4.6 ATTITUDE ESTIMATION PERFORMANCE VIA A LINEAR MULTIPLE FILTER ARCHITECTURE

The linear multiple model (LMM) filter is examined to pave the way for the Multiple Model Adaptive Estimation (MMAE) approach. It also serves as the baseline architecture to address the multiple sensor fusion of multiple star trackers.

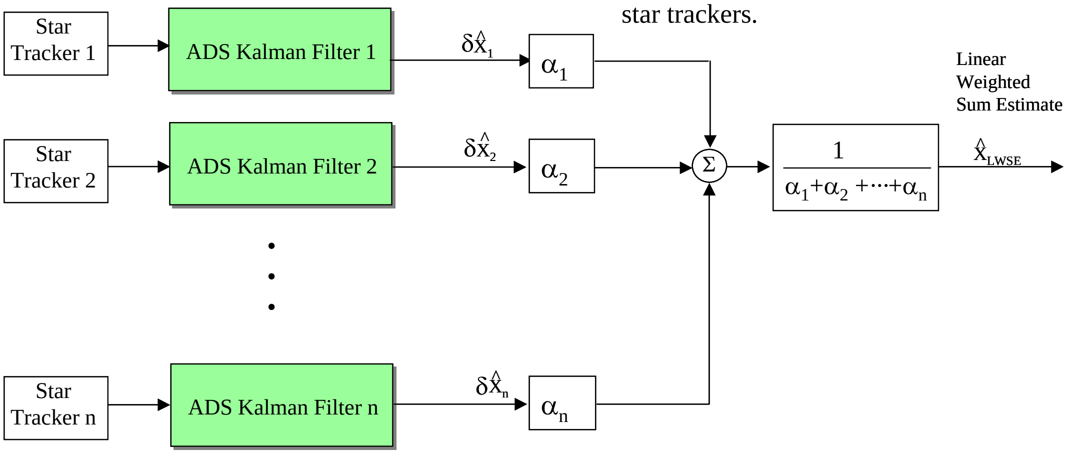

Figure 13: Linear Multiple Model Filter for Multiple Star Tracker Fusion

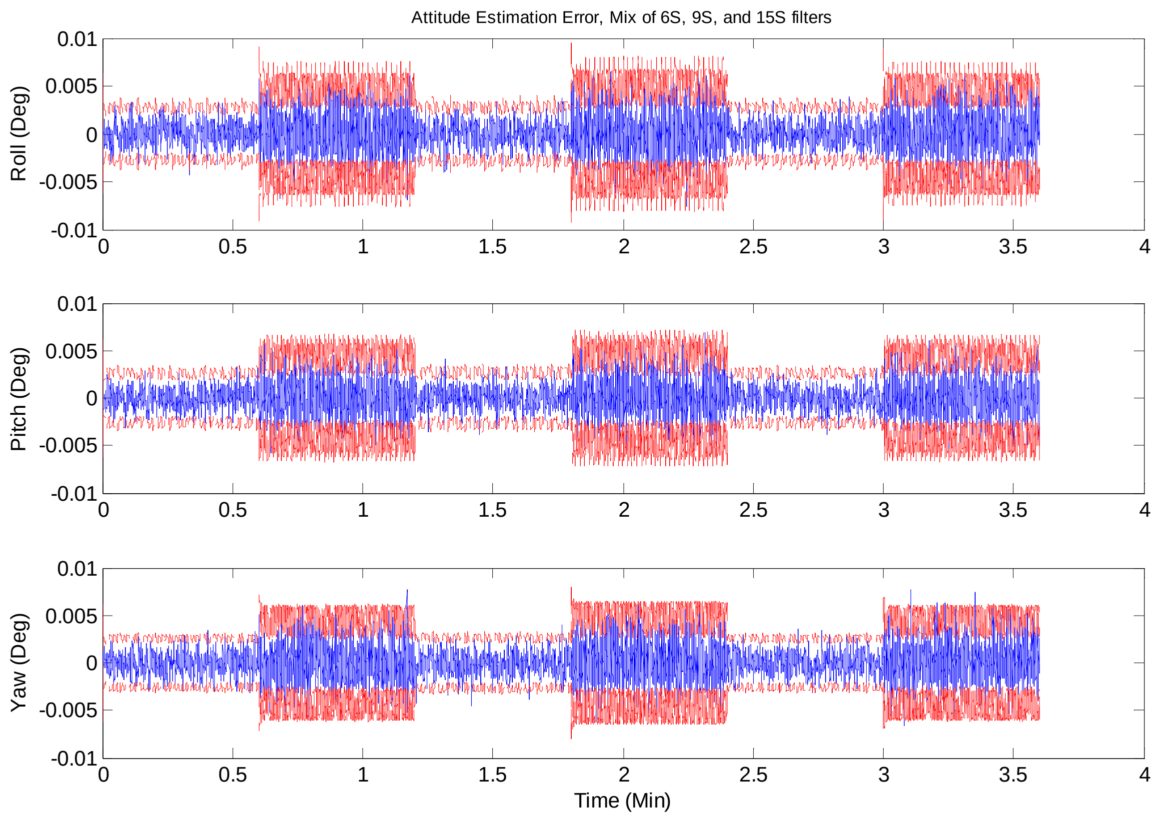

Figure 14: Attitude Estimation Via Linear Multiple Model Mixing (Fixed Coefficients) (1sig=[4.9 4.3 4.9] arcsecs, Enhanced Performance in all Axes Over Any Single EKF)

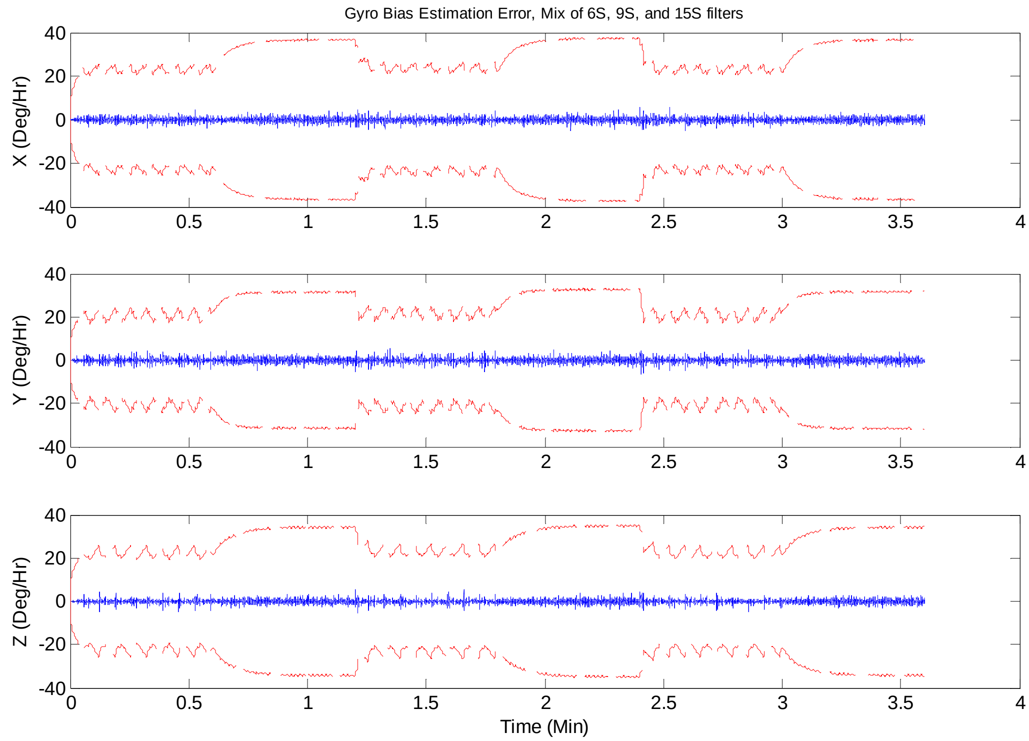

Figure 15: Gyro Bias Estimation Via Linear Multiple Model Mixing (Fixed Coefficients)

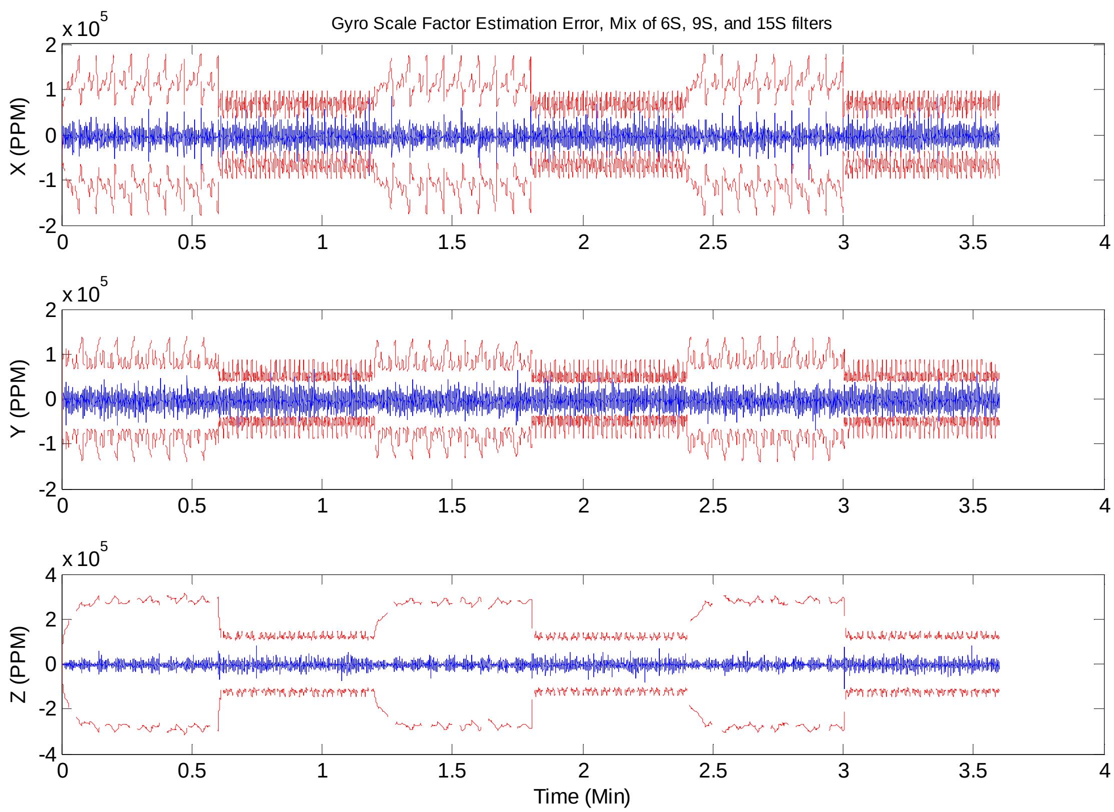

Figure 16: Gyro SF Estimation Via Linear Multiple Model Mixing (Fixed Coefficients)

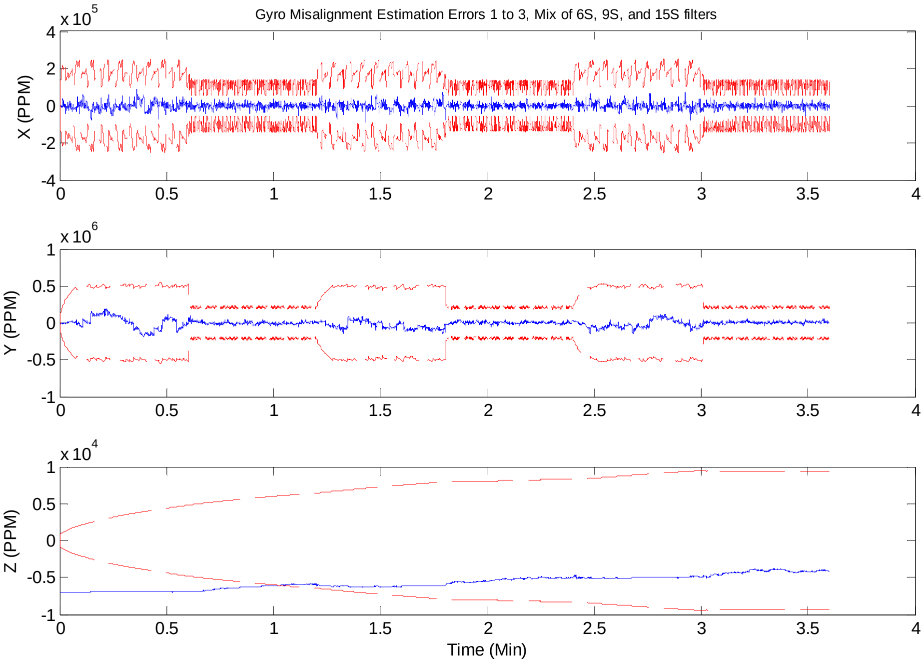

Figure 17: Gyro MA Estimation Via Linear Multiple Model Mixing (Fixed Coefficients)

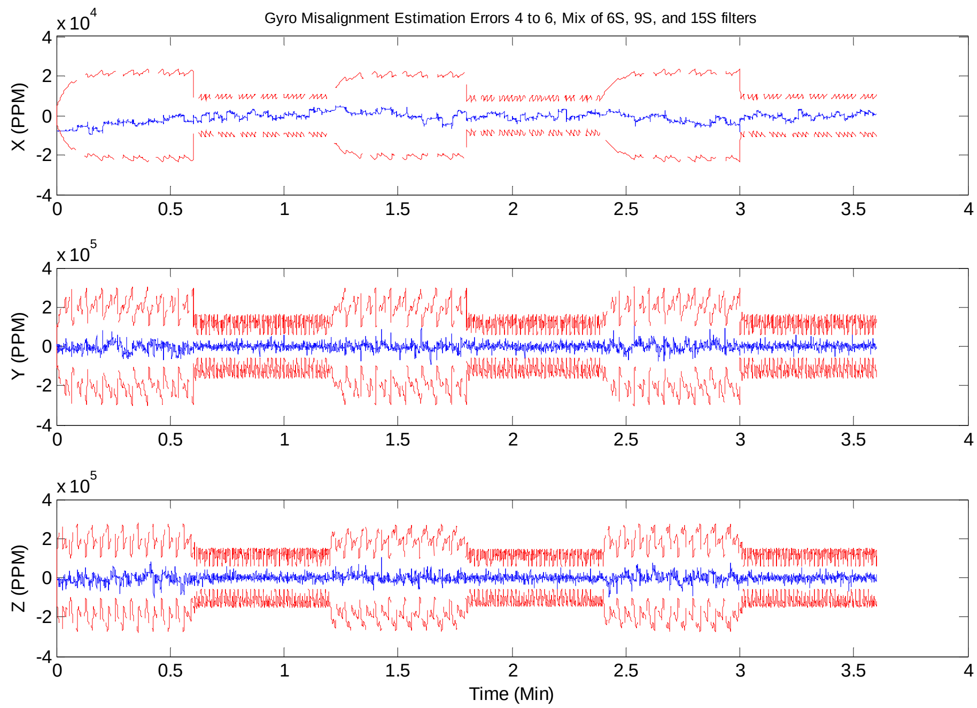

Figure 18: Gyro MA Estimation Via Linear Multiple Model Mixing (Fixed Coefficients)

Note that the coefficient α_i is selected to reflect the attitude quality provided by each star tracker (or sensor in general) that is mainly dictated by its mounting configuration and viewing geometry as well as orbit configuration/star observability variation. It is worth pointing out here that conventional ADS design procedure for multiple star tracker has not been able to address this issue. Again, for loose ADS attitude pointing knowledge type of missions, the conventional approach may allow ADS designers to comply with the mission requirements; however, for tighter attitude knowledge budget and higher precision type of missions, the proposed linear weighted correction using multiple attitude information from multiple sensors as presented in Figure 13 will definitely make a difference. Figures 14 to 18 present the overall performance improvement of the LMM when the following weighted coefficients α_i values are used for three EKFs (i.e., 6 state, 9 state and 15 state filters): $\alpha_1 = 0.2$; $\alpha_2 = 0.4$, and $\alpha_3 = 0.4$.

4.7 MULTIPLE MODEL ADAPTIVE ESTIMATION (MMAE) FILTERING FOR MULTIPLE SENSOR FUSION ARCHITECTURE

The linear multiple model filter design framework is now extended into an MMAE scheme wherein the pre-selected α_i coefficients now can be computed on-line using some adaptive computation scheme subject to a performance criterion. The MMAE baseline algorithm described in Section 4.0 is adopted here to enhance the performance of a typical multi-slewing multi-rate operating condition during imaging mode presented early on. The MMAE architecture applied to the multiple model ADS filter is depicted in Figure 19 wherein three ADS filter structures are employed to address the multi-rate/multi-mode situation. The fifteen-state ADS filter is the largest model that is implemented to fully address the attitude error and the gyro high order calibration of bias and fully populated misalignment matrix. The nine-state ADS filter model will address the attitude error and the gyro bias and symmetrical scale factor errors. Finally, the six-state ADS filter model consisting of attitude and gyro bias error is implemented to provide precision attitude determination in the low rate operating condition.

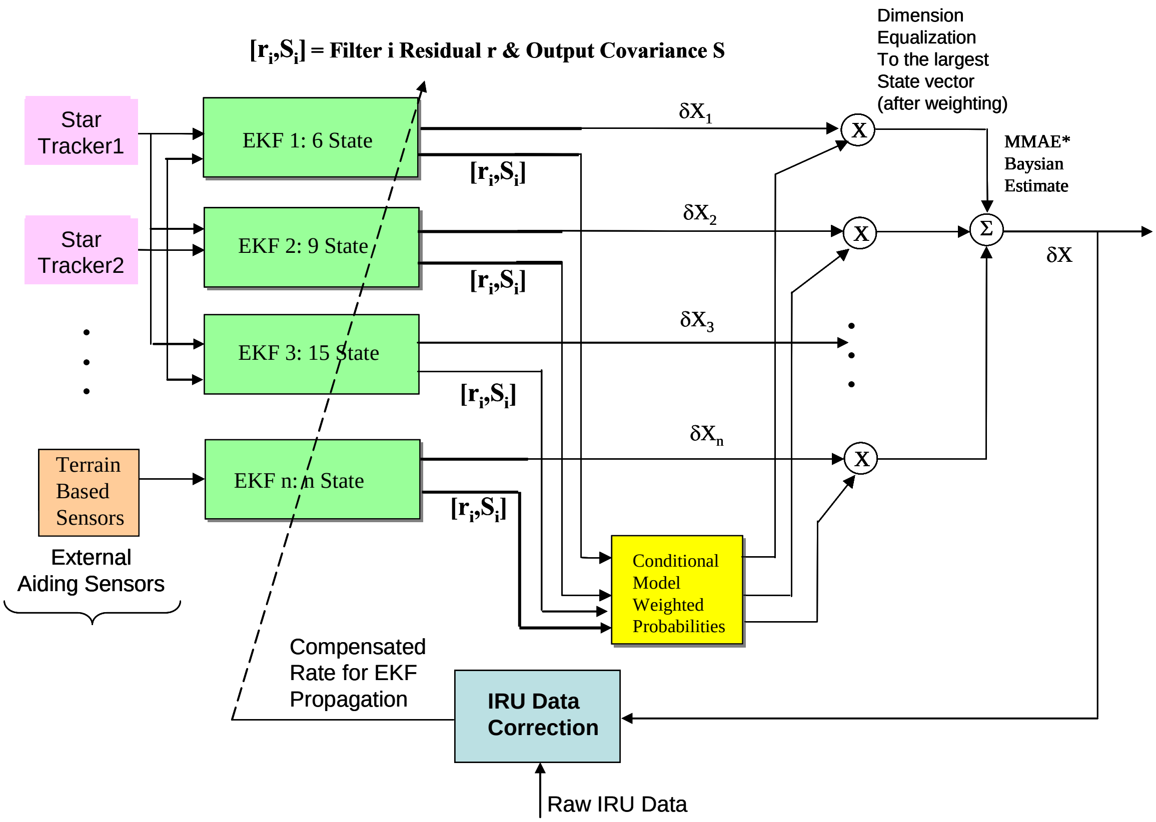

Figure 19: MMAE Architecture Suitable for Multiple Sensors Fusion

The multi-state mixing of three ADS filters is accomplished using the Bayesian blending method expressed as follows:

$$\delta\hat{x}^{Baysian}_{MMAE}(n+1) = \frac{\sum_{i=1}^{m} \delta\hat{x}_i(n+1)\cdot p_i(n+1)}{\sum_{i=1}^{m} p_i(n+1)} \qquad (31)$$

where m is the number of filter model in general. For the scope of this paper, m is set to 3. The conditional probabilities p_i are computed as:

$$p_i(n+1) = \frac{f_{z(n+1)|a,Z(n)}(z_i \mid a_i, Z_n)\, p_i(n)}{\sum_{j=1}^{m} f_{z(n+1)|a,Z(n)}(z_i \mid a_i, Z_n)\, p_j(n)} \qquad (32)$$

where

$$f_{z(n+1)|a,Z(n)}(z_i \mid a_i, Z_n) = \beta_i e^{[-0.5 r_i(n)^T [HPH^T + R]^{-1} r_i(n)} \qquad (33)$$

MMAE Mixing of 6 State and 9 State EKF Models

Figures 20 to 23 present the performance of the MMAE mixing using a single star tracker data for update to illustrate the benefits of the multiple models state mixing. With the state mixing of two EKF models via MMAE scheme, the performance and accuracy of the ADS solution are further improved beyond the traditional single EKF approach. Figures 20 to 23 illustrate the performance improvement offered by the MMAE approach. Both gyro bias and scale factor error estimates are now behaving extremely well and stay within the 3 sigma bound as compared to results generated by all previous cases, ranging from baseline single EKF to linear multiple model mixing.

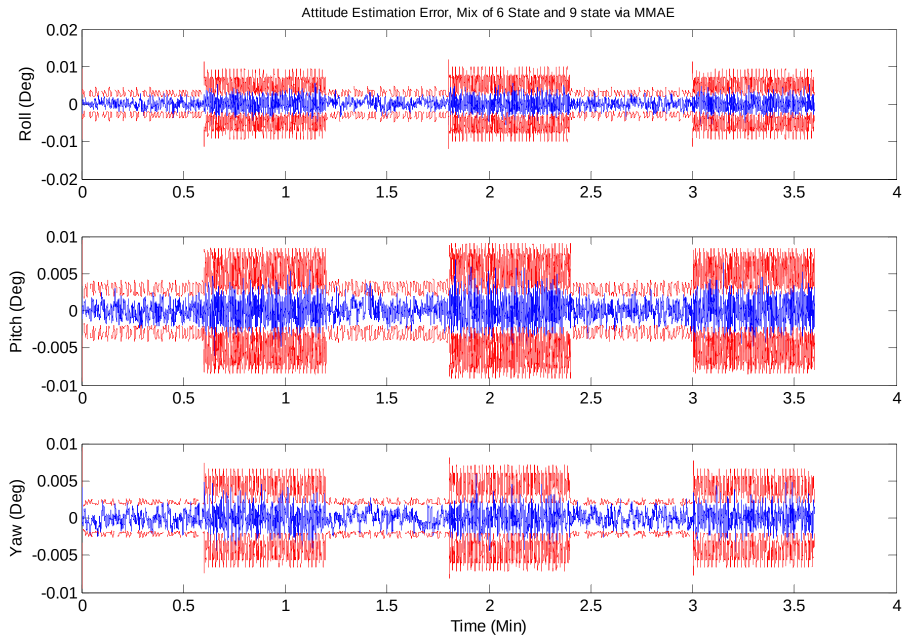

Figure 20: Attitude Performance Via MMAE Mixing
(1sig=[4.4 4.3 4.0] arcsecs, An Enhanced Performance over 15 state EKF & LMM Even with just a mixing of 6 state and 9 state EKFs via MMAE Mixing)

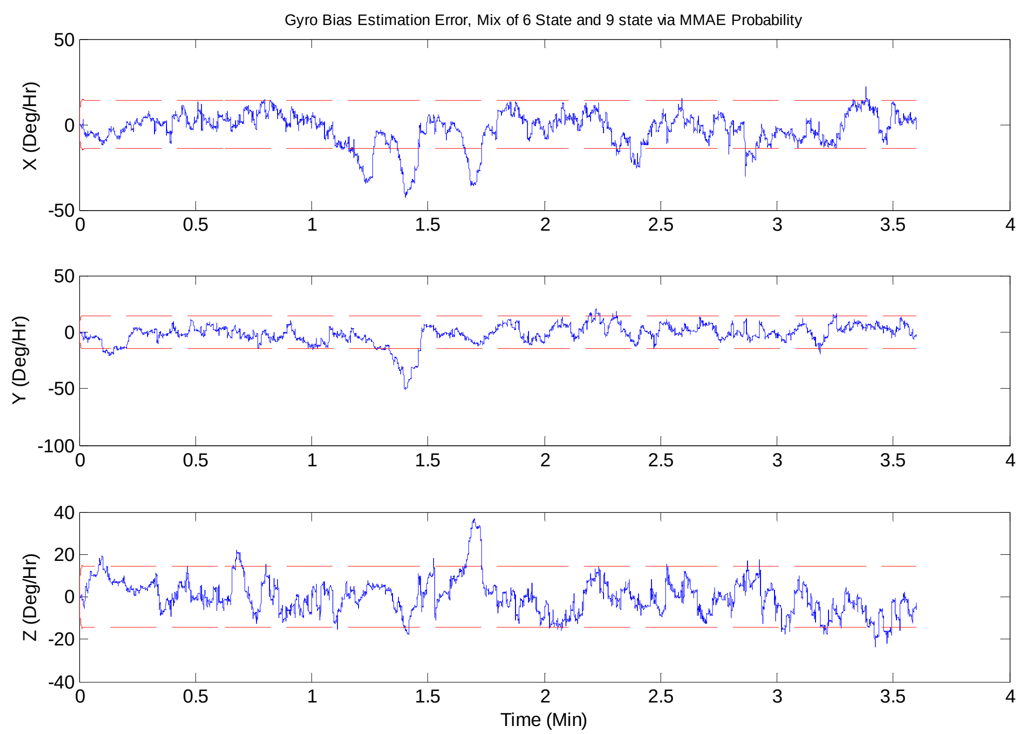

Figure 21: Gyro Bias Estimation Via MMAE Mixing

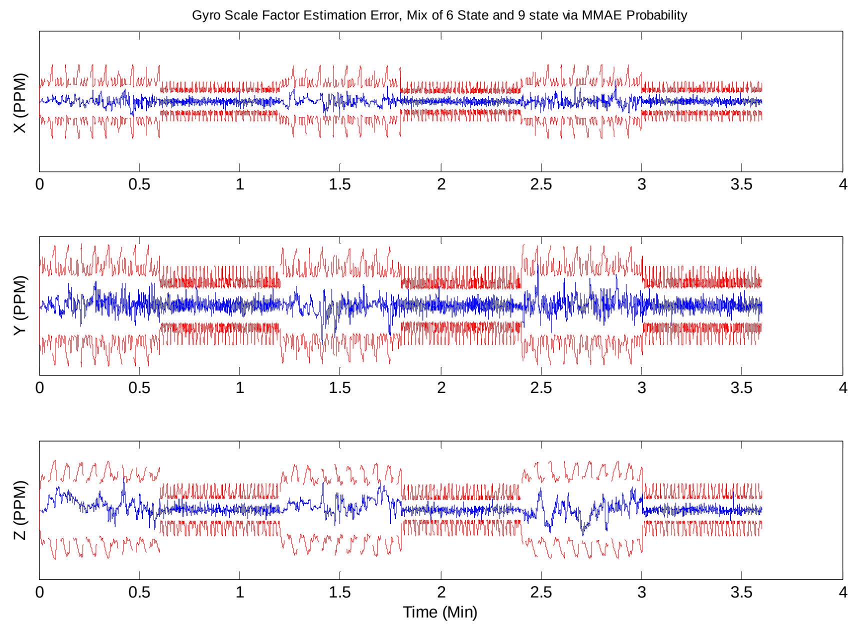

Figure 22: Gyro SF Estimation Via MMAE Mixing

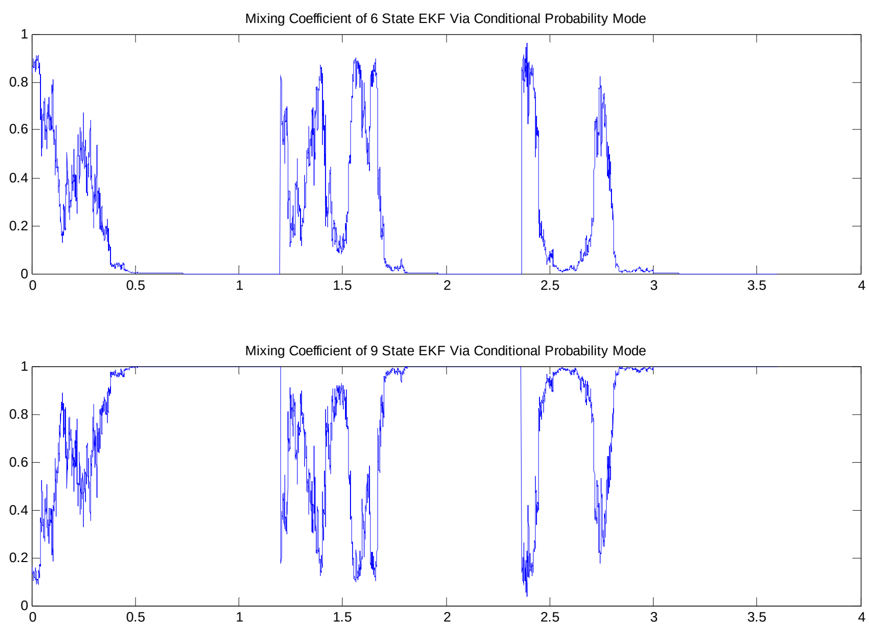

Figure 23: MMAE Dynamic Mixing Coefficients

Figure 23 illustrates the excellent on-line adaptation of MMAE mixing ability against system variation.

5.0 CONCLUSION

An adaptive filtering architecture via MMAE scheme is proposed to ameliorate the effect of gyro SF and MA errors at high rate operating condition and effectively maintain a precision attitude estimation performance while a traditional EKF scheme suffers for a same operating condition. The MMAE scheme is exploited to offer two primary design features: (1) on-board gyro noise estimation to update the EKF process noise *Q* matrix in real-time and (2) multiple EKF models mixing to provide the right fusion combination between various filter models' state vectors for a consistent attitude update at various rate magnitudes. The effectiveness of the proposed scheme is demonstrated via simulation. Due to time constraint and limited budget, the multi-sensors (e.g., two star trackers, IRU, and other update sensors like radar altimeter) fusion using the proposed MMAE has not been fully evaluated yet; however, the architecture itself, the mixing scheme (of a single tracker and an IRU), and the ability to adaptively compute the right *dynamic* mixing coefficient values for each filter presented in this paper strongly motivate us to continue our effort [9]. Further studies will continue examining its potential and evaluating its applicability of multi sensors mixing at higher fidelity of sensors models and more realistic high rate operating scenarios.

REFERENCES:

1. Lefferts, E. J., Markley, F. L., and Shuster, M. D., "Kalman Filtering for Spacecraft Attitude Estimation," *Journal of Guidance, Control, and Dynamics*, Vol. 5, No. 5, 1982, pp. 417–429.
2. Shuster, M. D., "A Survey of Attitude Representations," *Journal of the Astronautical Sciences*, Vol. 41, No. 4, 1993, pp. 439–517.
3. Markley, F.L., Crassidis, J.L., and Cheng, Y., "Nonlinear Attitude Filtering Methods," *AIAA Guidance, Navigation, and Control Conference*, San Francisco, CA, Aug. 2005, AIAA Paper #2005-5927.
4. Shuster, M. D., and Oh, S. D., "Three-Axis Attitude Determination from Vector Observations," *Journal of Guidance and Control*, Vol. 4, No. 1, 1981, pp. 70–77.
5. Crassidis, J.L., "Sigma-Point Kalman Filtering for Integrated GPS and Inertial Navigation," *AIAA Guidance, Navigation, and Control Conference*, San Francisco, CA, Aug. 2005, AIAA Paper #2005-6052.
6. Stengel, R.F., *Optimal Control and Estimation*, Dover Publications, New York, NY, 1994, pp. 402–407.
7. Cheng, Y., Markley, F.L., Oshman, Y., and Crassidis, J.L., "Averaging Quaternions," submitted to the *2007 AAS/AIAA Space Flight Mechanics Meeting*, Sedona, AZ, Jan.-Feb. 2007.
8. Lam, Q., Lakso, J., Hunt, T., and Vanderham, P., "Enhancing Attitude Estimation Accuracy Via System Noise Optimization," Presented at the *SPIE 2004*, Orlando, FL.
9. Lam, Q. M. and Crassidis, J. L., "Evaluation of a Multiple Model Adaptive Estimation Scheme for Space Vehicle's Enhanced Navigation Solution," to be Submitted to the AIAA GN&C Conference, Hilton Head, SC, 2007

BIOGRAPHY

Dr. Quang M. Lam is currently a Senior Scientist at Orbital Sciences Corporation. He received his MSEE, MSME, and BSME, all from Drexel University, in 1989, 1985, and 1983, respectively, and the Ph.D. in EE from Columbus University in 1999. Dr. Lam has a successful track record in technology development and new business initiatives. These include but are not limited to the following: (1) Global Precipitation Measurement (GPM) Avionics Package Study Award, (2) Precision Formation Flying Selection as partner with GSFC, (3) Stellar Inertial Attitude Determination System for NOAA GOES Weather Satellite Programs, (4) GN&C Lead for the Lunar Lander (Robotic Lunar Exploration Program), (5) winner of 8 SBIR programs, to name a few. Prior to joining Orbital, he has held many key positions in aerospace industry. These include GN&C Engineering Fellow at Raytheon, Chief Technologist at Swales Aerospace, VP of Applied Intelligent System Division at Welch Engineering, Ltd, and Sr. Attitude Control Subsystem Staff at Grumman. In addition to numerous technical reports and memos, has published 36 technical papers in GN&C and space technology development areas. His expertise and research interests include GPS/INS, ST/IRU based attitude determination, inertial based and vision-based mixing, adaptive filtering, system/parameter estimation and identification, adaptive controls, integrated guidance and control, and middleware technology applications to distributed and war-game simulation.

Dr. John Crassidis is an Associate Professor of Mechanical and Aerospace Engineering at the University at Buffalo (UB), State University of New York. He received his B.S., M.S., and Ph.D. in Mechanical Engineering from the State University of New York at Buffalo specializing in robust state estimation techniques and dynamics. Before joining UB in 2001, he held previous academic appointments at the Catholic University of America (1996-98) and Texas A&M University (1998-2000). He also held a position as a NASA Postdoctoral Research Fellow at Goddard Space Flight Center (1996-1998). While at NASA-Goddard he worked on a number of projects and research ventures, including: the application of a predictive filter scheme to determine the attitude of an actual spacecraft, the Solar Anomalous and Magnetospheric Particle Explorer (SAMPEX), using magnetometer measurements only; the development of contingency attitude filter designs for Tropical Rainfall Measurement Mission (TRMM) spacecraft; an investigation of hardware and software modifications to the Geostationary Operational Environmental Satellite (GOES) spacecraft; the development of robust control strategies for the Microwave Anisotropy Probe (MAP) spacecraft; and the development of efficient algorithms that determine the attitude and integer ambiguities from GPS signals. He also was the principal investigator of a new approach to determine air leaks on the International Space Station and his work has been highlighted through several national press associations and websites. Some of his current projects include relative navigation of UAVs using a novel sensor approach, ground tracking of vehicles incorporating trafficability reports, new methods in multiple-model adaptive estimation using autocorrelation methods, signal extraction from undersampled data, accurate derivative approximations using complex-step approaches, and novel methods for determining angular rates using star images without star identification.